Int. J. Heat Mass Transfer. Vol. 33, No. 3, pp. 529–541, 1990
Printed in Great Britain

0017–9310/90 $3.00 + 0.00

Combined heat and mass transfer in natural convection between vertical parallel plates with film evaporation

W. M. YAN and T. F. LIN

Department of Mechanical Engineering, National Chiao Tung University, Hsinchu, Taiwan 30050, R.O.C.

(*Received* 29 *December* 1988 *and in final form* 30 *June* 1989)

Abstract—A numerical analysis is carried out to investigate the effects of latent heat transfer, in association with the evaporation of a finite liquid film on the channel wall, on the natural convection heat and mass transfer. Results for heat and mass transfer rates are specifically presented for the systems with ethanol film evaporation and water film evaporation. The predicted results with the transport in the liquid film treated are contrasted with those with the transport in the liquid film untreated and show that the assumption of an extremely thin film is only valid for a system with small liquid mass flow rate. But for a system with a large liquid mass flow rate, the assumption becomes inappropriate.

1. INTRODUCTION

LATENT heat transfer associated with liquid film evaporation in natural convection flows driven by the combined buoyancy forces of heat and mass transfer resulting from the simultaneous presence of differences in temperature and variations in concentration are important in natural environments and engineering applications. Outstanding examples include double-diffusive convection in ocean flows, the simultaneous diffusion of metabolic heat and perspiration in controlling our body temperature especially on hot summer days, the cooling of a high temperature surface by coating it with phase-change material, and the evaporative cooling process for waste heat disposal.

Natural convection heat transfer in vertical open channel flows induced by the buoyancy of thermal diffusion alone has been examined in great detail [1–5]. The effects of mass diffusion on natural convection heat transfer have been widely studied for external flows [6–8] and internal flows [9–11]. As far as mixed convection flows are concerned, the influence of the wetted wall on the laminar mixed convection heat transfer in a vertical pipe is investigated in ref. [12]. While for forced convection heat and mass transfer, studies have been carried out for flows over a flat surface [13, 14] and a wedge [15].

The studies [10–15] just reviewed above all focus on the heat and mass transfer in the gas stream and neglect the liquid film thickness on the wall. The results thus produced are only good for a system with an extremely thin film. But in practical situations, the liquid film on the wall is finite in thickness, and thereby the influences of the momentum and energy transport in the liquid film on the heat and mass transfer in the gas flow should be considered in the analysis. Recently, Suzuki *et al.* [16], Baumann and Thiele [17], and Shembharkar and Pai [18] examined, respectively, the effects of finite film thickness on the heat and mass transfer in forced convection flows.

Despite the fact that the combined heat and mass transfer in natural convection between vertical parallel plates with finite film thickness is relatively important in engineering applications, it has not received much attention. The main objective of the present study is twofold: to check the suitability of the assumption of negligible film thickness in refs. [10, 11] and to investigate the momentum and heat transfer in the finite liquid film on the heat and mass transfer in natural convection flows.

2. ANALYSIS

The geometry of the system to be examined, as schematically shown in Fig. 1, is the vertical parallel plates with length ℓ and half channel width b. The channel walls are wetted by the thin liquid film with an inlet liquid temperature T_{fi}. The walls are kept at the same constant and uniform temperature, T_w. The air in the ambient is drawn into the channel by the resultant forces of thermal buoyancy, solutal buoyancy, and shearing force exerted by the falling film. As mentioned in refs. [10, 11], the induced flow in the channel may move upwards or downwards, depending on the direction of the resultant force (thermal buoyancy B_T, solutal buoyancy B_M and shear force τ_i). If the medium of the liquid film is water, the directions of these forces at different thermal conditions can be illustrated as follows.

(A) $T_w > T_0$

B_T (thermal buoyancy) : upward

B_M (solutal buoyancy) : upward

τ_i (shear force) : downward. (1)

NOMENCLATURE

B	liquid mass flow rate per unit periphery length at the inlet
b	half channel width
c_p	specific heat
c_{pa}	specific heat for air
c_{pv}	specific heat for vapour
D	mass diffusivity
$\tilde{D}$	wave mass diffusivity
d_g	damping function in gas side
d_ℓ	damping function in liquid side
f	wave frequency
Gr_M	Grashof number (mass transfer), $g(M_a/M_v-1)(w_r-w_0)b^4/\ell\nu_0^2$
Gr_T	Grashof number (heat transfer), $g(T_w-T_0)b^4/(\ell\nu_0^2T_0)$
g	gravitational acceleration
h_{fg}	latent heat of vaporization
ℓ	channel length
$\dot{m}_I''$	interfacial mass flux
M_a	molecular weight of air
M_r	dimensionless accumulated evaporation rate
M_v	molecular weight of vapour
Nu_ℓ	local Nusselt number (latent heat), equation (15)
Nu_s	local Nusselt number (sensible heat), equation (15)
$\overline{Nu}_s$	average sensible heat Nusselt number, $\int_0^\ell Nu_s\,dx/\ell$
Nu_x	interfacial local Nusselt number, Nu_s+Nu_ℓ
p	mixture pressure
p_I	partial pressure of vapour at gas–liquid interface
p_m	motion pressure (dynamic pressure), $p-p_0$
Pr	Prandtl number of the mixture
Pr_ℓ	Prandtl number of the liquid film
q_I''	total interfacial energy flux in gas side
$q_{\ell I}''$	interfacial latent heat flux in gas side (or net enthalpy flux), $\dot{m}_I''h_{fg}$
q_{sI}''	interfacial sensible heat flux in gas side, $[(\lambda+\tilde{\lambda})\partial T/\partial y]_{g,I}$
q_w''	heat transfer rate at channel wall
Ra	modified Rayleigh number, $Pr(Gr_T+Gr_M)$
Re_ℓ	liquid film Reynolds number, equation (32b)
Sc	Schmidt number
Sh	interfacial local Sherwood number
T	temperature
T_I	gas–liquid interface temperature
$T_{\ell i}$	inlet liquid film temperature
T_w	wall temperature
u	axial velocity
u_I	gas–liquid interface velocity
u_0	inlet axial velocity
v	transverse velocity
w	mass fraction of vapour
w_r	saturated mass fraction of vapour at T_w and p_0
w_I	mass fraction of vapour at gas–liquid interface
We	Weber number, equation (31)
x	coordinate in the flow direction
y	coordinate in the transverse direction.

Greek symbols

Γ	dimensionless surface tension parameter, equation (32a)
δ	local liquid film thickness
δ'	average wave amplitude
λ	molecular thermal conductivity
$\tilde{\lambda}$	wave thermal conductivity
μ	molecular dynamic viscosity
$\tilde{\mu}$	wave dynamic viscosity
ρ	density
τ_I	shear force at the gas–liquid interface.

Subscripts

a	air
g	mixture (air+ethanol vapour or air+water vapour)
I	condition at the gas–liquid interface
ℓ	liquid film
v	vapour
w	condition of wall
0	at ambient condition or inlet condition.

In this condition, we do not know the direction of the induced gas flow without the help of the experiment. Therefore, under this condition, we need to solve the full Navier–Stokes equations including the inlet and outlet effects. It seems that this type of computation is quite complex and will be considered in the near future.

(B) $T_w < T_0$

B_T (thermal buoyancy) : downward

B_M (solutal buoyancy) : upward

τ_I (shear force) : downward. (2)

Due to the shearing action of the falling film on the gas stream, the gas flow near the gas–liquid interface would move downwards. Therefore, if we can show that the gas flow induced by the buoyancy forces only (i.e. neglecting the effect of shear force τ_I) would move downwards, then the gas stream induced by the result-

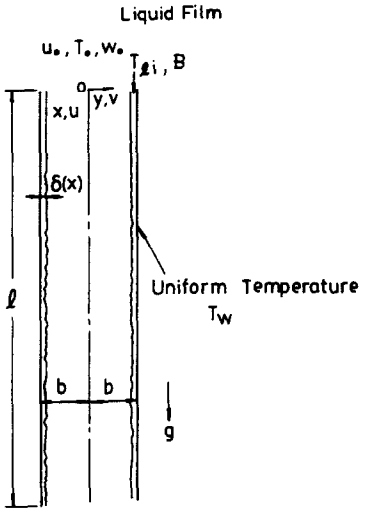

FIG. 1. Schematic diagram of the physical system.

ant forces would undoubtedly move downwards. As mentioned in refs. [10, 11], when the shear force τ_I on the gas stream is ignored, the direction of the induced gas flow can be approximately determined as follows:

$$\text{upward flow as } (Gr_T + Gr_M) > 0 \quad (3a)$$

$$\text{downward flow as } (Gr_T + Gr_M) < 0. \quad (3b)$$

Therefore, if $(Gr_T + Gr_M) < 0$, both the gas stream and falling film would move downwards. Otherwise, the flow reversal would occur in the gas stream.

If the liquid ethanol is considered for the film, the directions of thermal buoyancy, solutal buoyancy and interfacial shear force at different thermal conditions can also be summarized as follows.

(C) $T_w > T_0$

B_T : upward

B_M : downward

τ_I : downward. (4)

This condition is similar to that of case (B), equation (2).

(D) $T_w \leqslant T_0$

B_T : downward

B_M : downward

τ_I : downward. (5)

Clearly, the resultant force acts downwards. Thus the induced gas flow would move downwards.

To make the problem tractable by the boundary layer analysis, only the cases in which the induced gas flow is in the downward direction are chosen to examine the effects of the transport processes in the finite liquid film on the film evaporation in the natural convection flows. With this selection, the buoyancy induced heat and mass transfer in a vertical channel can then be solved by the boundary layer type governing equations.

2.1. *Governing equations*

(A) *Liquid film.* As a preliminary study consideration is given to a system with low liquid mass flow rate and hence the liquid film is assumed to flow laminarly. To facilitate the analysis, the inertia term in the momentum equation for the liquid film is neglected [17, 18], as compared to the diffusional term (viscous term). Therefore, the two-dimensional boundary layer flow in the liquid film is governed by the following conservation equations:

axial–momentum equation

$$0 = \frac{\partial}{\partial y}\left[(\mu_\ell + \tilde{\mu}_\ell)\frac{\partial u_\ell}{\partial y}\right] + \rho_\ell g \quad (6)$$

energy equation

$$\rho_\ell c_{p\ell} u_\ell \frac{\partial T_\ell}{\partial x} = \frac{\partial}{\partial y}\left[(\lambda_\ell + \tilde{\lambda}_\ell)\frac{\partial T_\ell}{\partial y}\right] \quad (7)$$

where $\tilde{\mu}_\ell$ and $\tilde{\lambda}_\ell$ are the wave viscosity and wave conductivity due to the interfacial wave effects which will be modelled in Section 3.

(B) *Gas flow.* The steady natural convection flows resulting from the combined buoyancy effects of thermal and mass diffusion can be described by the basic equations as:

continuity equation

$$\frac{\partial}{\partial y}(\rho u) + \frac{\partial}{\partial y}(\rho v) = 0 \quad (8)$$

axial–momentum equation

$$\rho u\frac{\partial u}{\partial x} + \rho v\frac{\partial u}{\partial y} = -\frac{\mathrm{d}p_m}{\mathrm{d}x} + \frac{\partial}{\partial y}\left[(\mu + \tilde{\mu})\frac{\partial u}{\partial y}\right] + g(\rho - \rho_0) \quad (9)$$

energy equation

$$\rho c_p u\frac{\partial T}{\partial x} + \rho c_p v\frac{\partial T}{\partial y} = \frac{\partial}{\partial y}\left[(\lambda + \tilde{\lambda})\frac{\partial T}{\partial y}\right] + \rho(D + \tilde{D})(c_{pv} - c_{pa})\frac{\partial T}{\partial y}\frac{\partial w}{\partial y} \quad (10)$$

concentration equation

$$\rho u\frac{\partial w}{\partial x} + \rho v\frac{\partial w}{\partial y} = \frac{\partial}{\partial y}\left[\rho(D + \tilde{D})\frac{\partial w}{\partial y}\right] \quad (11)$$

where $\tilde{\mu}$, $\tilde{\lambda}$, and $\tilde{D}$ are the wave viscosity, wave conductivity and wave mass diffusivity, respectively, which account for the effects of the interfacial waves on the transport processes in the gas flow. Notice that in the present study the thermophysical properties are taken to be variable. The detailed evaluation of them is given in refs. [21, 22]. It is worth noting that as the liquid film is regarded as extremely thin, the natural

convection heat and mass transfer in a vertical channel can be formulated in dimensionless form, as shown in our early investigations [10, 11]. The dimensionless temperature and interfacial Nusselt and Sherwood numbers are defined as [10, 11]

$$\theta = (T-T_0)/(T_w-T_0) \tag{12}$$

$$Nu_x = q_i''(4b)/[(T_w-T_0)k] \tag{13}$$

$$Sh = \dot{m}_i''(4b)/[\rho(w_i-w_0)D]. \tag{14}$$

According to the definition of the local Nusselt number in refs. [10, 11], the interfacial local Nusselt number can be expressed as

$$\begin{aligned} Nu_x &= Nu_s + Nu_f \\ &= q_{si}''(4b)/[(T_w-T_0)k] + q_{fi}''(4b)/[(T_w-T_0)k]. \end{aligned} \tag{15}$$

Obviously, as the wall temperature T_w equals the ambient temperature T_0, equations (12) and (15) become infinite. This occurs for some cases in the present study. Therefore, in this study the dimensional quantities are presented to illustrate the natural convection heat and mass transfer characteristics in the flow. But results for the Nusselt and Sherwood numbers, which are of value to thermal system design, will be presented for the cases with $T_w \neq T_0$.

2.2. *Boundary conditions*

At the inlet the flow is in the x-direction with uniform velocity, temperature, and mass fraction profiles

$$x = 0: \; u = u_0, \; T = T_0, \; w = w_0, \; p_m = -\rho u_0^2/2. \tag{16}$$

The condition at the centerline of the channel is

$$y = 0: \quad \frac{\partial u}{\partial y} = 0, \quad \frac{\partial T}{\partial y} = 0, \quad \frac{\partial w}{\partial y} = 0. \tag{17}$$

The conditions at the gas–liquid interface are

$$y = b-\delta(x): \quad u = u_i(x), \quad T = T_i(x), \quad w = w_i(x). \tag{18}$$

The conditions at the channel wall are

$$y = b: \quad u_f = 0, \quad T_f = T_w. \tag{19}$$

2.3. *Interfacial balances*

To make the problem tractable, the interface is assumed to be smooth. But the effects of the interfacial wave motion are accounted for by introducing the wave properties, $\tilde{\mu}$, $\tilde{\lambda}$, and $\tilde{D}$ into the boundary conditions and differential equations. The interfacial balances are described as follows:

velocity

$$u_i = (u)_{f,i} = (u)_{g,i} \tag{20}$$

temperature

$$T_i = (T)_{f,i} = (T)_{g,i} \tag{21}$$

shear stress

$$\tau_i = [(\mu+\tilde{\mu})(\partial u/\partial y)]_{f,i} = [(\mu+\tilde{\mu})(\partial u/\partial y)]_{g,i} \tag{22}$$

mass balance

$$\dot{m}_i'' = [\rho(D+\tilde{D})/(1-w_i)](\partial w/\partial y)_i \tag{23}$$

energy balance

$$[(\lambda+\tilde{\lambda})(\partial T/\partial y)]_{f,i} = [(\lambda+\tilde{\lambda})(\partial T/\partial y)]_{g,i} + \dot{m}_i'' h_{fg}. \tag{24}$$

It is noted that in equation (24) the terms on the right-hand side represent the interfacial sensible heat flux from the interface to the gas stream q_{si}'' and the net enthalpy flux to the interface due to latent heat transfer (film vaporization) q_f'', respectively. While the term on the left-hand side of equation (24) stands for the interfacial heat flux in the liquid side and is regarded as the total interfacial heat flux, q_i'' $(= q_{si}'' + q_{fi}'')$.

The interfacial mass fraction is obtained by assuming the gas–liquid interface to be in thermodynamic equilibrium [11]

$$w_i = M_v p_i/[M_a(p-p_i) + M_v p_i]. \tag{25}$$

3. WAVE MODEL

When the falling liquid film is disturbed so that the fluid particles are displaced from their original streamlines, two kinds of resulting forces—gravity and surface tension—can be called into play. The motion of the fluid brought by these restoring forces will not cease when the fluid particle has reached its original position of dynamic equilibrium but will overshoot the mark and requires the action of the restoring forces again. Thus wave motion is generated.

The surface waves on a falling liquid film normally appear at $Re_f > 20$ except for regions near the start of the flow. The waves appearing at the line of wave inception have a two-dimensional character with roughly sinusoidal-like wave fronts moving down the surface. These sinusoidal-like waves persist for a short distance but soon begin to distort. In the region of flow immediately following the sinusoidal-like wave, there are significant spatial variations in wavelength and dispersion characteristics [19].

Due to the complexity of the characteristics of wave motion, very few works have directly considered the influence of the interfacial waves on the transfer processes. To account for the effects of wave motion on the heat and mass transfer, a simple wave model for $\tilde{\mu}$ in parallel with the Prandtl–Kolmogorof hypothesis [16] is used. The wave viscosity for the liquid film is expressed as [16]

$$\tilde{\mu}_f = c_f \rho_f \delta'^2 f d_f \tag{26}$$

where δ' is the wave amplitude and f the wave fre-

quency. Since the wave-induced motion is damped out near the channel wall, a damping function d_f is used to set $\tilde{\mu}_f$ to zero near the channel wall.

The wave-induced motion is also expected to affect the gas flow near the interface. The effects are taken into account by introducing a wave viscosity $\tilde{\mu}_g$ defined as

$$\tilde{\mu}_g = c_g \rho_g \delta'^2 f d_g \tag{27}$$

where the values for c_f and c_g are carefully adjusted in the numerical computation. They are respectively chosen as 0.1 and 10 so as to make the magnitudes of the wave viscosities for the liquid and gas phases approximately equal to 10% of the corresponding molecular viscosity for each phase and to make the predicted results confirm the general perception that the existence of the interfacial wave can augment the heat and mass transfer rates by 10–20%. Similarly, a damping function d_g is also employed. In the present study the damping functions, d_f and d_g, are optimized via a number of experimentally computational runs. The detailed description is available in ref. [20]. The damping functions d_f and d_g are

$$d_f = 1 - \exp[-(b-y)/\delta] \tag{28a}$$

and

$$d_g = \exp[-5(b-\delta-y)/\delta]. \tag{28b}$$

During the experimentally computational runs, it is found that as the constants c_g and c_f are chosen to be zero (i.e. the effects of the wavy interface on the transports in the gas and liquid phases are neglected entirely), the predicted heat transfer rates in the gas stream are underpredicted by about 10–20%.

Since no systematical study of the wave parameters for the ethanol falling film exists in literature, the theoretical data of the wave parameters obtained by Hirshburg and Florschuetz [21] for the water falling film are used. Empirical relations for the wave frequency f and wave amplitude δ' fitting their theoretical results are

$$\begin{aligned} f &= 86.7\, We^{0.371327}\ (\mathrm{s}^{-1}), \\ &\quad \text{if } We \leqslant 0.0264443 \\ &= 71.79\, We^{0.319413}\ (\mathrm{s}^{-1}), \\ &\quad \text{if } We > 0.0264443 \end{aligned} \tag{29}$$

and

$$\begin{aligned} \delta' &= 4.1236 \times 10^{-4} We^{0.5505}\ (\mathrm{m}), \\ &\quad \text{if } We \leqslant 0.038357 \\ &= 1.5340 \times 10^{-4} We^{0.2472}\ (\mathrm{m}), \\ &\quad \text{if } We > 0.038357 \end{aligned} \tag{30}$$

where the Weber number, We, is defined as

$$We = (Re_f/4)^{5/3}/\Gamma. \tag{31}$$

Here the surface tension parameter Γ and liquid film Reynolds number Re_f are defined as

$$\Gamma = 0.6736219(\sigma/\rho_f \nu_f^{4/3}) \tag{32a}$$

and

$$Re_f = 4B/\mu_f. \tag{32b}$$

In the above equations B is the liquid mass flow rate per unit periphery length at the inlet and σ the surface tension of the liquid film. The temperature dependencies of surface tension for water and ethanol are available in refs. [22, 23].

It should be emphasized that in the present study the Weber number has been assumed to be the governing dimensionless group for the falling film waves. Therefore, the wave parameters of the ethanol falling film can be approximately estimated from those of the water falling film. This assumption was verified by the theoretical results of Massot *et al.* [24] and Gollan and Sideman [25]. They found that the Weber number We is the determining dimensionless group for falling film waves.

Notice that the wave properties $\tilde{\lambda}$ and $\tilde{D}$, are estimated by introducing the wave Prandtl number $\tilde{Pr}$ and wave Schmidt number $\tilde{Sc}$. In the present study, both $\tilde{Pr}$ and $\tilde{Sc}$ are taken to be 1. This means that the effects of interfacial waves on the heat and mass transfer are identical to the momentum transfer.

4. SOLUTION METHOD

In view of the impossibility of obtaining an analytic solution as indicated in the literature survey, the conjugated problem defined by the governing equations, equations (6)–(11), is solved by the finite-difference numerical method. In the present study the matching conditions imposed at the gas–liquid interface, equations (22) and (24), to ensure the continuities of shear stress and heat flux are cast in backward difference for $(\partial\varphi/\partial y)_g$ and forward difference for $(\partial\varphi/\partial y)_f$ with φ denoting u or T. Therefore, the governing equations in the gas flow and liquid film can be solved simultaneously.

Because the flow under consideration is a boundary-layer type, the solution for equations (6)–(11) can be marched in the downward direction. A fully implicit numerical scheme in which the axial convection is approximated by the upstream difference and the transverse convection and diffusion terms by the central difference is employed to transform the governing equations into finite-difference equations. Each system of the finite-difference equations forms a tridiagonal matrix equation which can be efficiently solved by the Thomas algorithm [26]. For a given condition, a brief outline of the solution procedures is described as follows.

(1) Guess an inlet velocity u_0.

(2) For any axial location, guess the values of $(\mathrm{d}p_m/\mathrm{d}x)$, $\dot{m}_i''$, and δ, and solve the finite-difference forms of equations (6)–(11) for u, θ, and w.

(3) Integrating the continuity equation of the gas stream numerically to find v

$$v = -\frac{1}{\rho}\frac{\partial}{\partial x}\int_0^y \rho u \, dy. \tag{33}$$

(4) Check the satisfaction of the overall conservation of mass in the gas flow and liquid film. If the following criteria

$$\left|\int_0^{b-\delta} \rho u \, dy - \left[\rho u_0 (b-\delta_0) + \int_0^x \dot{m}_1'' \, dx\right]\right| \Big/ \rho u_0 b < 10^{-4} \tag{34a}$$

and

$$\left|B - \left[\int_{b-\delta}^{b} (\rho u \, dy)_l + \int_0^x \dot{m}_1'' \, dx\right]\right| \Big/ B < 10^{-4} \tag{34b}$$

are met, then test the convergence of the velocity, temperature, and concentration fields. If the maximum relative errors for u, T, and w between two consecutive iterations satisfy the criteria

$$\frac{\max|u_{i,j}^n - u_{i,j}^{n-1}|}{\max|u_{i,j}^n|} < 10^{-4} \tag{35a}$$

$$\frac{\max|T_{i,j}^n - T_{i,j}^{n-1}|}{\max|T_{i,j}^n|} < 10^{-4} \tag{35b}$$

$$\frac{\max|w_{i,j}^n - w_{i,j}^n|}{\max|w_{i,j}^n|} < 10^{-4} \tag{35c}$$

the solution for the current axial location is complete. Now if equations (35) are not simultaneously met, repeatedly solve the finite-difference equations for u, T, and w in the gas stream and the liquid film and use equation (33) to get v until the condition specified in equations (35) is fulfilled. If equations (34) are not satisfied, adjust dp_m/dx, $\dot{m}_1''$, and δ and repeat procedures (2)–(4) for the current axial location.

(5) Procedures (2)–(4) are successively applied to every axial location from the channel entrance to the exit.

(6) Check whether the exit pressure p_m is zero. If not, guess a new inlet velocity u_0 by the Newton–Raphson method and repeat procedures (2)–(6). If yes, the solution is complete.

It is noted that the thickness of the liquid film decreases with x due to the film evaporation. Therefore, during the downward marching at each iteration the numerical grid is rearranged to ensure that one of the grid points is located at the gas–liquid interface.

To obtain enhanced accuracy in the numerical computations, grids are chosen to be nonuniform in the streamwise direction and in the transverse direction to account for the drastic variations of u, T, and w in the regions near the inlet and gas–liquid interface. Several grid sizes are tested and a comparison of the results among the computations for a typical case is given in Table 1. It is noted that the difference in the local interfacial heat flux q_1'', for the computation by using the $101 \times 81 \times 21$ and $201 \times 161 \times 41$ grids are always less than 2%. Accordingly, the computation by the $101 \times 81 \times 21$ grid is sufficient to understand the heat and mass transfer characteristics in the gas flow and liquid film. To further check the adequacy of the numerical scheme, the results for the limiting case of natural convection in a vertical channel without the film evaporation are obtained. Excellent agreement between the present predictions and those of Aung *et al.* [2] was found.

5. RESULTS AND DISCUSSION

In order to investigate the effects of the liquid flow rate and thermal conditions on the characteristics of heat and mass transfer, ten cases given in Table 2 are selected for the computation. All the above cases are based on a vertical channel of width 3 cm. It is apparent in Table 2 that both ethanol film and water film are considered in the present study. But for most cases the ethanol film is considered. Moreover, the heat and mass transfer Grashof numbers, Gr_T and Gr_M, for all cases satisfy the condition

$$Gr_T + Gr_M < 0. \tag{36}$$

This means that the combined buoyancy due to thermal and mass diffusion is in the downward direction, and both the gas flows and falling liquid film would then undoubtedly move downwards. Therefore, with the boundary layer approximations adopted the cases listed in Table 2 can then be solved by the boundary-layer equations. It should be emphasized that not all the values for the non-dimensional groups, e.g. Pr, Sc, Gr_T, etc., can be arbitrarily assigned. In fact, they are interdependent for a given mixture under certain specific conditions. In light of practical situations, T_0, T_w, T_{∞}, B, and ℓ are selected as the independent physical parameters. All the non-dimensional parameters can then be evaluated (Table 2). As indicated in Table 2, the liquid Prandtl number is of the order of 10. As expected, the liquid Prandtl number would be of the order of 1 as the liquid film temperature is relatively high.

To check the suitability of the assumption of the liquid film being extremely thin in refs. [10, 11], the developments of the velocity, temperature, and mass fraction for a typical case predicted with finite liquid film thickness and zero film thickness are contrasted in Figs. 2–4, respectively. For clear illustration the velocity and temperature profiles near the interface are specifically plotted in the insets in Figs. 2 and 3. An overall inspection of these figures reveals that the distributions of u, T, and w for zero film thickness resemble those for finite film thickness. Careful observation, however, discloses that the differences between these two treatments (i.e. considering finite film thickness and neglecting film thickness) are substantial, especially in the region close to the gas–liquid inter-

Table 1. Comparison of local interfacial heat flux q_i'' for various grid arrangements for case IV

x/ℓ	$I \times J \times L$ 201 × 161 × 41	101 × 161 × 21	101 × 81 × 21	51 × 81 × 11	51 × 41 × 11
0.047	470.60	470.20	473.95	492.81	497.55
0.1026	333.02	334.73	337.24	339.97	338.92
0.2005	248.0	250.25	252.30	246.78	247.22
0.4086	182.17	182.09	185.70	182.12	184.78
0.6521	147.81	147.72	149.16	146.23	149.61
0.9117	125.63	125.24	126.66	123.81	127.20

I, total number of grid points in the x-direction.
J, total number of grid points placed in the y-direction in the gas side.
L, total number of grid points placed in the y-direction in the liquid side.

Table 2. Values of major parameters for various cases

Case	T_w	T_{fi}	T_0	B	Gr_T	Gr_M	Pr	Sc	Pr_f
					Ethanol film				
I	40	40	20	0.005	148.82	−205.83	0.710	1.311	12.27
II	40	40	20	0.01	148.82	−205.83	0.710	1.311	12.27
III	40	40	20	0.02	148.82	−205.83	0.710	1.311	12.27
IV	20	20	20	0.005	0.0	−71.65	0.710	1.311	16.22
V	20	20	20	0.01	0.0	−71.65	0.710	1.311	16.22
VI	20	20	20	0.02	0.0	−71.65	0.710	1.311	16.22
VII	20	20	40	0.01	−110.45	−56.71	0.706	1.304	16.22
VIII	20	20	40	0.02	−110.45	−56.71	0.706	1.304	16.22
					Water film				
IX	20	20	40	0.005	−110.45	15.19	0.706	0.509	6.97
X	20	20	40	0.04	−110.45	15.19	0.706	0.597	6.97

Units for parameters: T in °C; B in kg m^{-1} s^{-1}.
In the present study the channel length ℓ is 1 m while the channel width b is 0.03 m.

face. Because the characteristics of heat and mass transfer are particularly important at the interface, as expected, the differences in these two predictions in the local interfacial heat and mass transfer rates would be important.

It is clearly seen in Fig. 2(a) that the velocity of the gas stream at the channel entrance is relatively uniform. But as the flow goes downstream, the profile becomes distorted with the maximum velocity away from the channel centre. This feature can be made plausible by noting the fact that because the combined buoyancy forces near the interface acts in the flow direction of the liquid film, the effect of the thermal and solutal buoyancy is then to increase the velocity near the interface, and meanwhile to reduce the velocity at the centre to maintain the overall mass

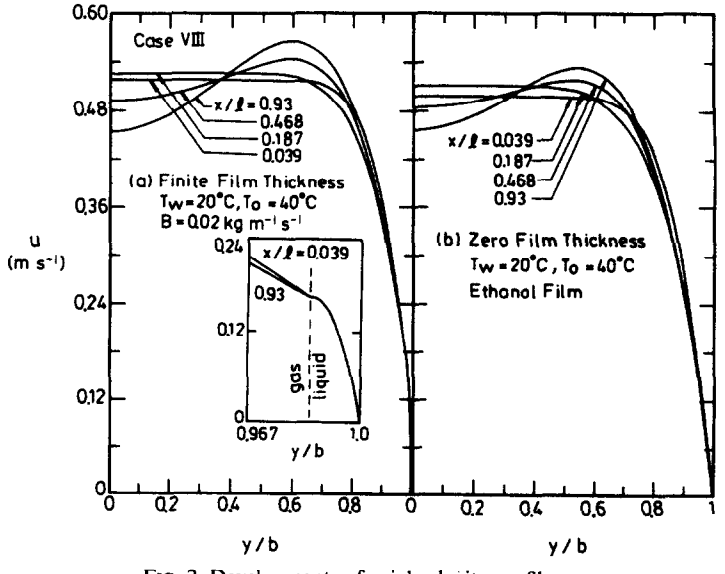

FIG. 2. Developments of axial velocity profiles.

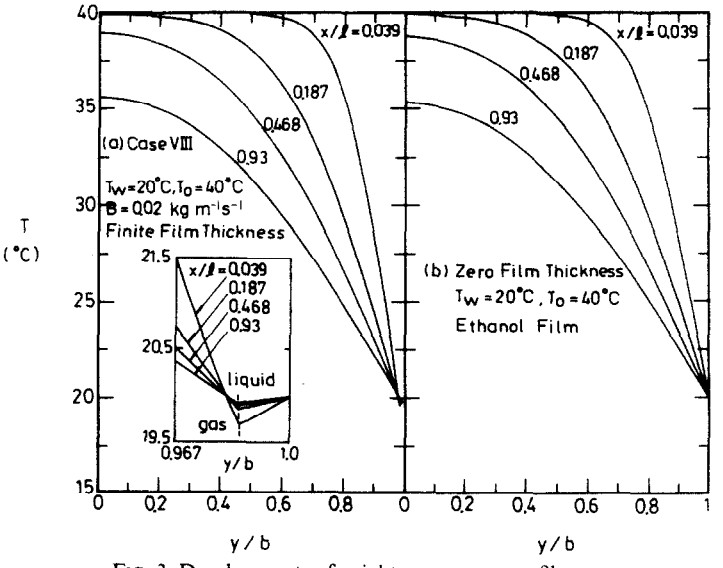

FIG. 3. Developments of axial temperature profiles.

balance. Moreover, comparing the corresponding curves between Figs. 2(a) and (b) shows that the induced velocity in the gas stream is slightly underpredicted when the transport in the liquid film is neglected in the analysis. This is due to the neglect of the positive shearing effect of the falling film on the gas flow as the film is untreated. It is also worth noting in the inset in Fig. 2(a) that the flow velocity in the liquid film is nearly parabolic.

Figure 3 shows the axial developments of temperature in the gas stream and liquid film. As mentioned above, the differences in the corresponding curves between those predicted with transport in the film considered (Fig. 3(a)) and those without (Fig. 3(b)) are small in the core region of the gas flow. This implies that the existence of the falling film does not affect the temperature distributions of the gas stream away from the film so much. But near the gas–liquid interface, the deviations between them are rather significant, as indicated in the inset in Fig. 3(a). It is apparent from the inset that in the gas side the gas temperature monotonically decreases with y down to the gas–liquid interface. This indicates that the direction of sensible heat transfer in the gas side is from the gas flow to the interface. But in the liquid side the temperature increases with y, indicating that the heat transfer in the liquid is from the liquid to the interface although $T_0 > T_w$. Apparently, the sensible heat transfer in the gas flow and liquid film all goes to the interface and is absorbed by the film vaporization, a latent heat transfer process. The energy absorption by the film vaporization is so effective that the gas and liquid near the interface are below the wall temperature 20°C. It is also noted in the inset that the liquid temperature varies almost linearly with y. This result is in line with the assumption made in the Nusselt type analysis, that is, the liquid film temperature varies linearly with y due to the small thickness of the liquid film.

Consistent with the vaporization of the ethanol film, the mass fraction of the ethanol vapour shown in Fig. 4 increases gradually as the gas moves downstream. Careful scrutiny of Figs. 4(a) and (b) indicates that the concentration boundary layers predicted with the assumption of zero film thickness develop a little more rapidly than those for finite film thickness.

In the study of combined heat and mass transfer over a falling film, the wall heat transfer rate is one of the most important quantities. Depicted in Fig. 5 are the local wall heat flux distributions q''_w. For comparison purposes, the gas–liquid interfacial heat flux q''_i is also included in this figure. Comparison of the solid line for case VII with that for case VIII indicates that the larger the liquid flow rate, the larger the wall heat flux. This confirms the general perception that in the falling film the heat transfer between the liquid and heated wall is more effective in the flow with a larger liquid mass flow rate [27]. In addition, it is also interesting to compare the distributions of the wall heat flux q''_w with the total interfacial heat flux q''_i $(= q''_{si} + q''_{li})$. Comparison shows that near the entrance (i.e. small x/ℓ) the difference between them is relatively large, indicating the significant longitudinal convection energy transfer in the liquid film at small x/ℓ. As the liquid moves further downstream the difference becomes small, especially for the case with a small liquid flow rate (see case VII). This result suggests that downstream the axial convection is negligible and the temperature field is fully developed, as evident from the inset in Fig. 3(a). Thus heat input from the wall completely transfers to the interface across the film. If we define the region between the inlet and the location where the interfacial heat flux is 95% of the wall heat flux to be the thermal entrance region, we can then draw the conclusion from Fig. 5 that the shorter thermal entrance length is experienced for the cases with a smaller liquid mass flow rate. This also implies that for large liquid mass flow rate the

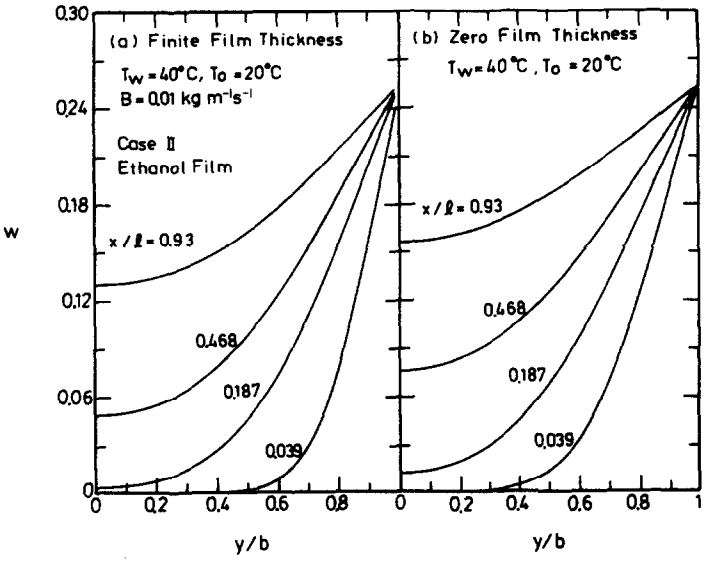

FIG. 4. Developments of axial mass-fraction profiles.

assumption of heat transfer being thermally fully developed in the whole liquid film is not appropriate. It is also worth noting in Fig. 5 that the larger the liquid mass flow rate, the larger the total interfacial heat flux (by comparing cases VII and VIII).

To study the relative contributions of heat transfer through the sensible and latent heat exchanges between the liquid film and gas flow, both the interfacial sensible heat flux q''_{sI} and latent heat flux q''_{lI} in the gas side are presented in Figs. 6(a) and (b). Regarding q''_{sI} curves, substantial deviations exist among various cases. The positive values of q''_{sI} for case II means that the direction of heat transfer is from the interface to the gas stream, vice versa for the case with negative q''_{sI} for case VII. The reason for the outcome of the positive or negative q''_{sI} can be readily realized if we check Table 2. For case II T_w is larger than T_0, which in turn results in a positive q''_{sI}.

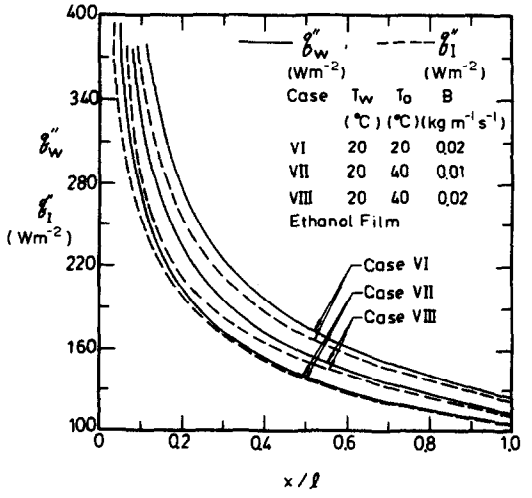

FIG. 5. Comparisons of local wall and total interfacial heat transfer rates.

Similarly, for case VII ($T_w < T_0$) q''_{sI} is negative. As for case V, because T_w is identical to T_0, as expected, q''_{sI} is rather small.

Attention is now turned to the distributions of q''_{lI} (Fig. 6(b)). According to the results in Fig. 6(b), the system with a higher wall temperature shows a higher value for q''_{lI} (by comparing cases II and V or cases II and VII). This is brought about by the larger latent heat transport in connection with the larger liquid

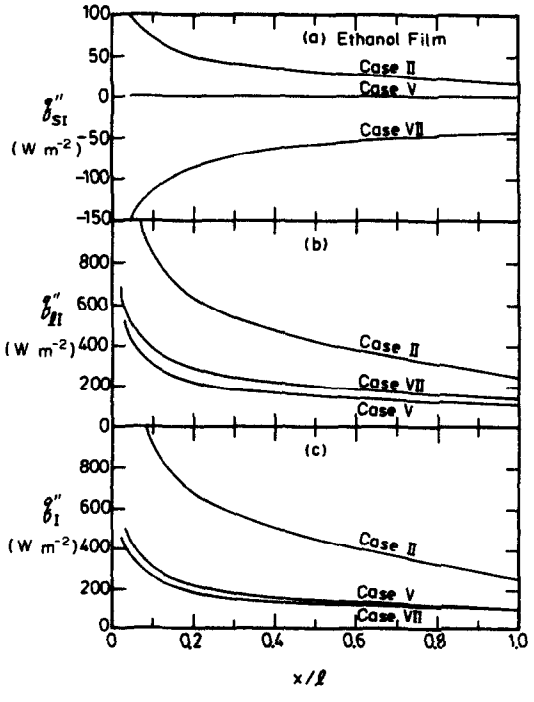

FIG. 6. Distributions of local heat transfer rates in the gas side along the channel: (a) interfacial sensible heat transfer; (b) interfacial latent heat transfer; (c) total interfacial heat transfer.

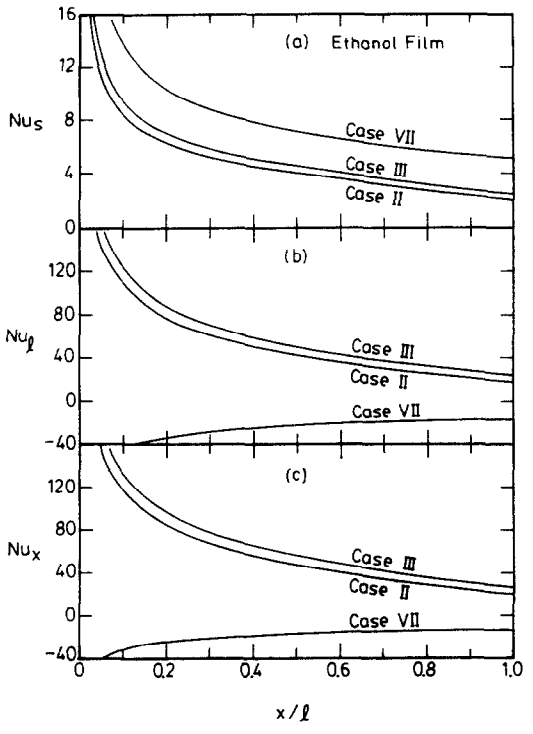

FIG. 7. Local Nusselt number distributions for ethanol film evaporation: (a) sensible heat; (b) latent heat; (c) overall Nusselt numbers.

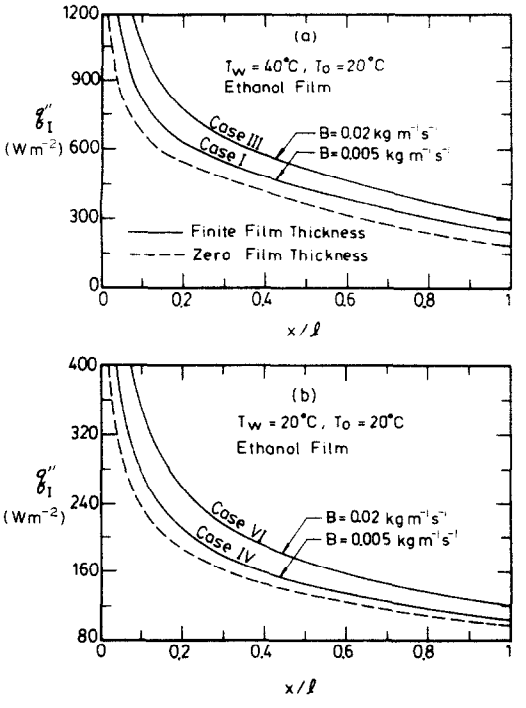

FIG. 8. Comparisons of total interfacial heat transfer rates between finite liquid film thickness and zero film thickness.

film evaporation for a higher T_w. By comparing the ordinate scales of Figs. 6(a) and (b), it is apparent that the magnitude of q''_l is much larger than that of q''_{sl}, indicating that heat transfer resulting from latent heat exchange is much more effective. Also clearly seen in Fig. 6(b) is the influence of the ambient temperature T_0 on the variation of q''_l. Shown in Fig. 6(c) are the local distributions of the total interfacial heat flux q''_I ($= q''_{sl} + q''_l$). It is distinctly observed in Fig. 6 that q''_I for case VII is always positive, while the values of q''_{sl} for the same case are negative. This means that the direction of interfacial heat transfer q''_I is in opposition to that of sensible heat transfer q''_{sl} in the gas side. This also illustrates the superiority of film cooling in which the liquid film is used as a heat barrier to protect the channel wall from the hot air stream.

In Fig. 7, the local Nusselt numbers are presented for some cases with $T_w \neq T_0$. Regarding the sensible heat Nusselt number in Fig. 7(a), only slight differences exist among various cases. While for the latent heat Nusselt number (in Fig. 7(b)), the deviations among cases are rather substantial. The negative values of Nu_l for case VII result directly from the definition of Nu_l, equation (15). For $T_w < T_0$ in case VII, Nu_l is negative since q''_l is positive. In other words, a negative Nu_l simply indicates that the direction of the latent heat exchange is opposed to that of the sensible heat exchange. These results suggest that for $T_w > T_0$ both Nu_s and Nu_l increase with the liquid flow rate.

Comparisons are made in Fig. 8 to check the suitability of the assumption of an extremely thin film in the analysis by examining the axial distributions of the total interfacial heat flux predicted by including the transport in the finite liquid film and by ignoring it for the cases with $T_w = 30$ and 20°C at different liquid mass flow rates B. It is apparent that q''_I calculated with zero film thickness is smaller than that calculated with finite film thickness. Besides, the differences between them increase with the liquid mass flow rate B. This is to say that the assumption of an extremely thin film is a limiting case and is valid for the system with a small B. As the liquid mass flow rate is large, especially for a system with a turbulent falling liquid film, the assumption becomes inappropriate.

It is interesting to investigate the influences of the thermal conditions and liquid mass flow rate on the interfacial mass evaporation rate. The predicted mass evaporation rate $\dot{m}''_I$ is presented in Fig. 9. In congruence with the discussion mentioned above, the interfacial mass evaporation rate is larger for the case with a higher T_w. Comparing cases II and III shows that the larger the liquid mass flow rate, the larger the mass evaporation rate.

The variations of local Sherwood number Sh, shown in Fig. 10, resembles that of Nu_s because Pr and Sc are of the order of 1 ($Pr = 0.7$ and $Sc = 1.3$). It is found in Fig. 10 that a higher Sh results for the system with lower T_w and higher T_0. This is due to the larger combined buoyancy forces (i.e. larger $Gr_T + Gr_M$).

The amount of ethanol vapour added to the gas

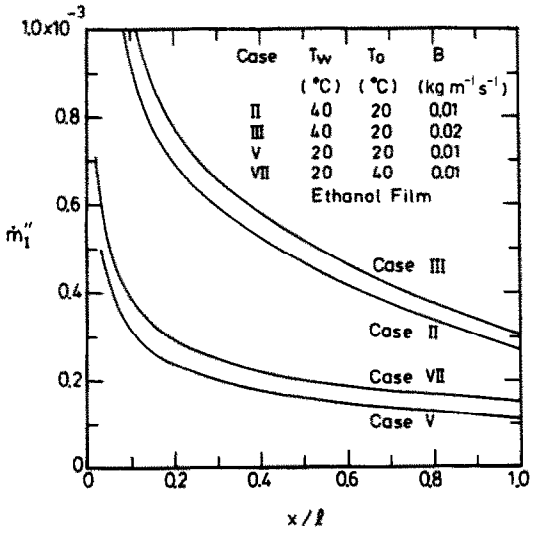

FIG. 9. Local interfacial mass evaporation rate along the channel.

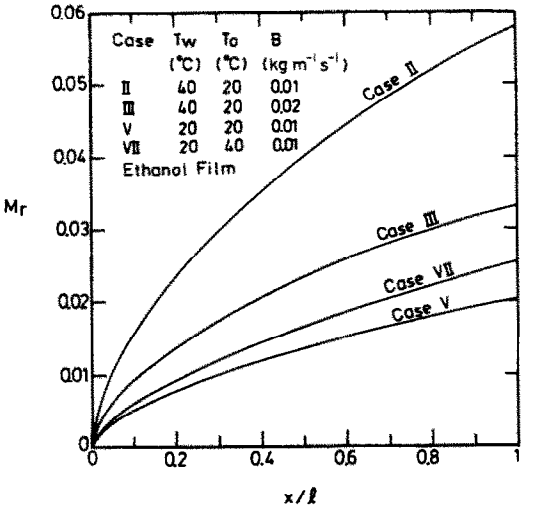

FIG. 11. Distributions of the dimensionless accumulated evaporation rate.

stream due to film vaporization is important in improving our understanding on the mass transfer rate. To this end, a non-dimensional accumulated mass evaporation rate is introduced

$$M_r = \frac{\text{evaporating mass flow rate}}{\text{inlet liquid mass flow rate}} = \int_0^x \dot{m}_1'' \, dx/B. \quad (37)$$

The distributions of M_r for various cases are presented in Fig. 11. Again larger film vaporization is observed for a system with a higher T_w. It is also worth noting that the largest dimensionless accumulated mass evaporation rate at $x/\ell = 1$ is less than 6%. This implies that the variations of the film thickness along the channel are small. The dryout of the liquid film does not occur in the present study.

A close inspection on the q_1'' distributions for ethanol film in Fig. 8 indicates that a 400% increase in the film flow rate results in about a 20–25% increase in q_1''. This also holds true in the results for the water film in Fig. 12. Therefore, the interfacial heat flux is not very sensitive to the film flow rate.

After examining heat and mass transfer with the ethanol film evaporation, attention is turned to the effects of the water film on the heat and mass transfer in a vertical channel. Shown in Fig. 12 are the axial distributions of the total interfacial heat flux in the gas side. For comparison purposes, both the predicted results with the transports in the finite film treated and those with the transport untreated are plotted together. It is clearly seen that neglecting momentum and heat transfer in the film underpredicts the interfacial heat flux. Additionally, the deviations in q_1'' become large as the liquid mass flow rate increases. This trend is similar to that of an ethanol film (see Fig. 8).

In Fig. 13, the average sensible heat Nusselt number is plotted against a modified Rayleigh number which accounts for the combined buoyancy forces of thermal and mass. Meanwhile, the liquid mass flow rate effect is incorporated into the average sensible heat Nusselt number. The corresponding correlation is given as

$$\overline{Nu_s}/\sqrt{(1+B/0.05)} = -0.0007635Ra^2 + 0.1683Ra - 0.4276 \quad (38)$$

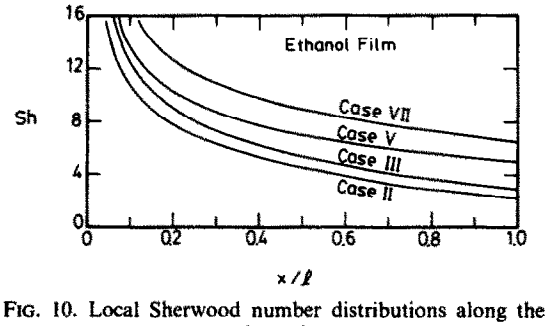

FIG. 10. Local Sherwood number distributions along the channel.

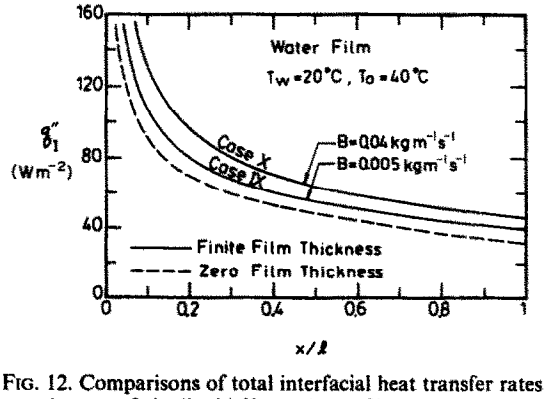

FIG. 12. Comparisons of total interfacial heat transfer rates between finite liquid film and zero film thickness.

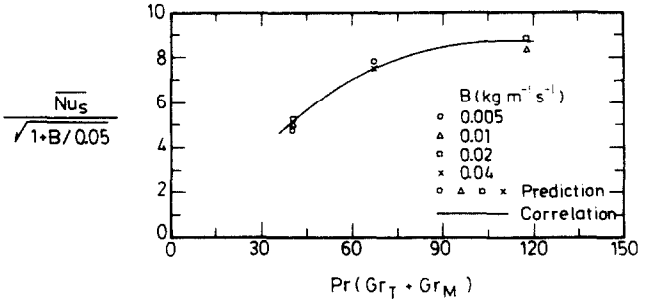

FIG. 13. Variations of the average sensible heat Nusselt number with the modified Rayleigh number.

where the modified Rayleigh number is defined as

$$Ra = Pr(Gr_T + Gr_M). \quad (39)$$

6. CONCLUSION

The nature of laminar natural convection heat and mass transfer in a vertical plate channel with film evaporation has been numerically studied with momentum and heat transfer in the liquid film treated. The influences of the system temperature and liquid flow rate on the momentum, heat, and mass transfer in both the liquid film and the gas stream are investigated in great detail. A brief summary of the major results is given below.

(1) Heat transfer between the interface and gas flow is dominated by the transport of latent heat in association with the vaporization of the liquid film.

(2) The existence of the falling film on the axial developments of the velocity, temperature and concentration in the core region of the gas stream is small. But near the gas–liquid interface, the influence of the falling film on the gas flow is rather substantial.

(3) The assumption of an extremely thin film thickness is a limiting condition and is only valid for the system with a small liquid mass flow rate. As the liquid mass flow rate is large, the assumption becomes inappropriate.

It is recognized herein that the results presented above are good for laminar wavy films, i.e. $Re_l < 1600$ [19, 27]. While as the liquid Reynolds number exceeds 1600, the predicted results by the present mathematical model become inappropriate because the film flow is turbulent [19, 27].

To the best knowledge of the authors, there does not exist a related experimental work on natural convection heat and mass transfer with film evaporation in the open literature. Due to its importance in engineering applications, the present authors are currently conducting an experimental study about the natural convection heat and mass transfer with film evaporation [28]. In ref. [28], the most pressing question encountered in the experimental run is to maintain the symmetrical and uniform film thickness on the walls. These experimental results will be reported later.

Acknowledgement—The financial support of this research by the engineering division of National Science Council of Taiwan, R.O.C., through contract NSC77-0401-E009-10 is greatly appreciated.

REFERENCES

1. J. R. Bodoia and J. F. Osterle, The development of free convection between heated vertical plates, *J. Heat Transfer* **84**, 40–44 (1962).
2. W. Aung, L. S. Fletcher and V. Sernas, Developing laminar free convection between vertical flat plates with asymmetric heating, *Int. J. Heat Mass Transfer* **15**, 2293–2308 (1973).
3. H. Akbari and T. R. Borgers, Free convection laminar flow within the Trombe wall channel, *Sol. Energy* **22**, 165–174 (1979).
4. A. Writz and R. J. Stutzman, Experiments on free convection between vertical plates with symmetric heating, *J. Heat Transfer* **104**, 501–507 (1982).
5. E. M. Sparrow and L. F. A. Azevedo, Vertical-channel natural convection spanning between the fully-developed limit and the single-plate boundary-layer limit, *Int. J. Heat Mass Transfer* **28**, 1847–1857 (1985).
6. W. M. Gill, E. D. Casal and D. W. Zeh, Binary diffusion and heat transfer in laminar free convection boundary layers on a vertical plate, *Int. J. Heat Mass Transfer* **8**, 1135–1151 (1965).
7. T. S. Chen and C. F. Yuh, Combined heat and mass transfer in natural convection along a vertical cylinder, *Int. J. Heat Mass Transfer* **23**, 451–460 (1979).
8. M. Hason and A. S. Mujumdar, Coupled heat and mass transfer in natural convection under flux condition along a vertical cone, *Int. Commun. Heat Mass Transfer* **11**, 157–172 (1984).
9. T. S. Lee, P. G. Parikh, A. Acrivos and D. Bershader, Natural convection in a vertical channel with opposing buoyancy forces, *Int. J. Heat Mass Transfer* **25**, 499–511 (1982).
10. C. J. Chang, T. F. Lin and W. M. Yan, Natural convection flows in a vertical open tube resulting from combined buoyancy effects of thermal and mass diffusion, *Int. J. Heat Mass Transfer* **29**, 1543–1552 (1986).
11. W. M. Yan, T. F. Lin and C. J. Chang, Combined heat and mass transfer in natural convection between vertical parallel plates, *Wärme- und Stoffübertr.* **23**, 69–76 (1988).
12. T. F. Lin, C. J. Chang and W. M. Yan, Analysis of combined buoyancy effects of thermal and mass diffusion on laminar forced convection heat transfer in a vertical tube, *J. Heat Transfer* **110**, 337–344 (1988).
13. L. C. Chow and J. N. Chung, Evaporation of water into a laminar stream of air and superheated steam, *Int. J. Heat Mass Transfer* **26**, 373–380 (1983).
14. J. Schroppel and F. Thiele, On the calculation of momentum, heat, and mass transfer in laminar and turbulent

boundary layer flows along a vaporizing liquid film, *Numer. Heat Transfer* **6**, 475–496 (1983).
15. C. H. Wu, D. C. Davis, J. N. Chung and L. C. Chow, Simulation of wedge-shaped product dehydration using mixtures of superheated steam and air in laminar flow, *Numer. Heat Transfer* **11**, 109–123 (1987).
16. K. Suzuki, Y. Hagiwara and T. Sato, Heat transfer and flow characteristics of two-component annular flow, *Int. J. Heat Mass Transfer* **26**, 597–605 (1983).
17. W. M. Baumann and F. Thiele, Heat and mass transfer in two-component film evaporation in a vertical tube, *Proc. 8th Int. Heat Transfer*, San Francisco, Vol. 4, pp. 1843–1848 (1986).
18. T. R. Shembharkar and B. R. Pai, Prediction of film cooling with a liquid coolant, *Int. J. Heat Mass Transfer* **29**, 899–908 (1986).
19. A. E. Dukler, Characterization, effects and modeling of the wavy gas–liquid interface, *Prog. Heat Mass Transfer* **6**, 207–234 (1972).
20. W. M. Yan, Buoyancy induced heat and mass transfer in vertical channel flows, Ph.D. Thesis, Department of Mechanical Engineering, National Chiao Tung University, Hsinchu, Taiwan, January (1989).
21. R. I. Hirshburg and L. W. Florschuetz, Laminar wavy-film flow: Part I, hydrodynamic analysis, *J. Heat Transfer* **104**, 452–458 (1982).
22. T. Fujii, Y. Kato and K. Mihara, Expression of transport and thermodynamic properties of air, steam and water, Sei San Ka Gaku Ken Kyu Jo, Report No. 66, Kyu Shu Dai Gaku, Kyu Shu, Japan (1977).
23. *JSME Data: Thermophysical Properties of Fluids*. The Japan Society of Mechanical Engineers (1983).
24. C. Massot, F. Iraani and E. N. Lightfoot, Modified description of wave motion in a falling film, *A.I.Ch.E. Jl* **12**, 445–455 (1966).
25. A. Gollan and S. Sideman, On the wave characteristics of falling films, *A.I.Ch.E. Jl* **15**, 301–303 (1969).
26. S. V. Patankar, *Numerical Heat Transfer and Fluid Flow*, Chap. 6. Hemisphere/McGraw-Hill, New York (1980).
27. S. M. Yih, Modeling heat and mass transfer in wavy and turbulent falling liquid films, *Wärme- und Stoffübertr.* **21**, 373–381 (1987).
28. T. F. Lin, Heat transfer enhancement through latent heat transfer in natural convection—III, Report for NSC-77-0401-E009-10, Taiwan (1989).

TRANSFERT DE CHALEUR ET DE MASSE EN CONVECTION NATURELLE ENTRE PLAQUES PARALLELES VERTICALES AVEC EVAPORATION EN FILM

Résumé—On conduit une analyse numérique pour étudier les effets du transfert de chaleur latente, en association avec l'évaporation d'un film liquide sur la paroi du canal, sur le transfert de chaleur et de masse en convection naturelle. Des résultats sont présentés pour des systèmes avec évaporation de film d'éthanol et de film d'eau. Les résultats du calcul montrent que l'hypothèse d'un film extrêmement mince est valide seulement pour un système avec un faible débit-masse de liquide. Mais pour un système avec un grand débit-masse de liquide, l'hypothèse n'est pas appropriée.

GEKOPPELTER WÄRME- UND STOFFÜBERGANG BEI FILMVERDAMPFUNG IN NATÜRLICHER KONVEKTION ZWISCHEN SENKRECHT ANGEORDNETEN PARALLELEN PLATTEN

Zusammenfassung—Es wird der Einfluß der Phasenänderung auf den Wärme- und Stoffübergang bei natürlicher Konvektion für den Fall numerisch untersucht, daß an der Kanalwand ein Flüssigkeitsfilm endlicher Dicke verdampft. Ergebnisse werden für die Verdampfung von Ethanol und Wasser angegeben. Die Rechenergebnisse mit und ohne Berücksichtigung von Transportvorgängen im Film werden einander gegenübergestellt. Der Vergleich zeigt, daß die Annahme eines sehr dünnen Films nur für kleine Flüssigkeitsmassenströme gerechtfertigt ist. Für Systeme mit großen Flüssigkeitsmassenströmen ist die Annahme ungeeignet.

СЛОЖНЫЙ ТЕПЛО- И МАССОПЕРЕНОС ПРИ ЕСТЕСТВЕННОЙ КОНВЕКЦИИ МЕЖДУ ВЕРТИКАЛЬНЫМИ ПАРАЛЛЕЛЬНЫМИ ПЛАСТИНАМИ С ПЛЕНОЧНЫМ ИСПАРЕНИЕМ

Аннотация—Численно анализируется влияние фазового перехода вследствие испарения жидкой пленки конечной толщины на стенке канала на свободноконвективный тепло- и массоперенос. Представлены данные по скорости тепло- и массопереноса при использовании этилового спирта, а также воды. Проведено сопоставление результатов расчета переноса с учетом и без учета теплопереноса в жидких пленках, и показано, что приближение тонкой пленки справедливо лишь для системы с малым массовым расходом жидкости. В случае же системы с большим массовым расходом жидкости упомянутое приближение неприменимо.